ELSEVIER

International Journal of Mass Spectrometry 214 (2002) 327–337

International Journal of Mass Spectrometry

www.elsevier.com/locate/ijms

Energy distributions of secondary ions sputtered from aluminium and magnesium by Ne^+, Ar^+ and $O_2{}^+$: a comprehensive study☆

A. Tolstogouzov[a,*], S. Daolio[a], C. Pagura[a], C.L. Greenwood[b]

[a] *Istituto di Polarografia ed Elettrochimica Preparativa (IPELP-CNR), Corso Stati Uniti 4, 35127 Padova, Italy*
[b] *Hiden Analytical Ltd., 420 Europa Boulevard, Warrington WA5 7UN, UK*

Received 30 October 2001; accepted 19 December 2001

Abstract

The energy distributions of positive and negative secondary ion species produced by 5 keV Ne^+, Ar^+ and $O_2{}^+$ ion bombardment at 30° to polycrystalline aluminium and magnesium targets have been studied. The measurements were carried out in a small solid angle along the surface normal, without extracting ions into the mass–energy analyser. The most probable and average energies along with the widths of the distributions were tabulated; essential features of the spectra were interpreted in the terms of a linear collision cascade model with a knock-on contribution. Three energy sub-ranges with appreciable different energy power dependence E^{-s}, which could approximate the experimental curves, were revealed for both Al^+ and Mg^+ atomic ions within a wide energy range $E_{mp} < E < 1000$ eV. Nearly all the energy spectra of negative secondary ions demonstrated complex structure, with two distinct peaks, caused by impurity species with different binding energies. (Int J Mass Spectrom 214 (2002) 327–337)

Keywords: Aluminium; Energy distribution; Ion sputtering; Magnesium; Mass–energy analysis; Secondary ion emission

1. Introduction

Though the majority of particles emitted from a surface under a keV ion-beam bombardment is in the neutral state (ground or exited), investigation of energy distributions (EDs) of secondary ions remains a topical issue because it enables an insight into the mechanisms of sputtering and ionisation processes occurring on the surface. To date, plenty of such studies have been done (see, e.g. [1–11] and references cited therein). In our paper, we are not about to discuss in detail their results, but want to stress here that, in fact, reliable energy spectra measurements are a very complicated problem [12,13]. They should be carried out under meaningful and well defined experimental conditions, above all, with a small (and constant) angular acceptance and without any extraction of the ions into mass–energy analyser by accelerating electric fields. This concept is not novel, but only a very limited number of ED studies [8–10] have been fulfilled under aforesaid conditions. The typical method for measuring energy distributions in SIMS instruments involves adjustments of the sample bias. This method results in a considerable distortion of the distributions, especially at low and moderate (less than 100 eV) secondary ion energy. As a consequence, such ED data are not suited for a direct comparison with theory.

☆ Partially presented at the 19th International Conference on Atomic Collisions in Solids (ICACS-19), Paris, France, 29 July–3 August 2001.

* Corresponding author. E-mail: alexander@ipelp.pd.cnr.it.

1387-3806/02/$20.00
PII S1387-3806(02)00523-7

This has motivated the present work, aimed to study the kinetic energy distributions of different secondary ion species (positive and negative) emitted into a small solid angle ($\Omega \sim 10^{-4}$ sr) along the normal to the surface by bombarding polycrystalline Al and Mg samples with 5 keV Ne^+, Ar^+ and $O_2{}^+$ primary ions. The measurements have been carried out with the sample at a fixed (ground) potential, without any extracting fields between sample and analyser. Energy distributions were measured for $M^{+(-)}$, M^{2+}, $M_n{}^+$ ($n = 2$, 3), $MO_m{}^{+(-)}$ ($m = 2$, 3) secondary ions, where M is Al or Mg, and for some positive and negative secondary ion impurities. The most probable energy, E_{mp}, the average energy, E_{avr}, the width, $\Delta E_{0.5}$, of the energy distributions and the parameter s of the energy power dependence E^{-s} have been determined for each secondary ion species.

2. Experimental

In the following, we will outline the essential parts of our installation, which were constructed and manufactured by IPELP-CNR, Italy, for studying ion–surface interaction phenomena [14–16]. The versatile system measures energy-resolved mass spectra and mass-resolved energy distributions of both positive and negative ions, and operates in SIMS, mass-resolved ion-scattering spectrometry (MARISS) and residual gas analysis (RGA) modes.

The pivotal element of the system is the EQS 1000 Mass Energy Analyser produced by Hiden Analytical [17]; its schematic configuration is shown in Fig. 1.

The extraction optics (1) includes two lenses whose operation is dependent on the type of particles sampled. Electronic modifications allowed the extraction voltages to be referenced to ground or floated at a given potential. A simplified schematic of the voltage reference diagram is shown in Fig. 1.

For SIMS trace elemental and depth profiling analyses the extraction electrodes are set to a high voltage to accept secondary ions from the sample with a range of angles and energy distributions. When running ED measurements or mass-resolved ion scattering experiments it is important to place a target into the equipotential region, which excludes any perturbation of the ion trajectories. A similar approach is widely used for the study of ion–surface collisions at chemically relevant primary energies (1–100 eV) [18–20], but as mentioned above, is not a generally accepted method for ED measurements at keV energy range.

The internal electron impact ionisation source (2), which is situated immediately after the extraction optics, consists of two oxide coated iridium filaments on opposing sides of a radially symmetric cage. The source can be employed for standard residual gas analysis or configured for electron attachment ionisation**.** In the scope of these investigations, only externally generated ions were considered, so the source region of the EQS was held at a potential (labelled *energy* in Fig. 1) corresponding to the sampled ion energy, providing a field free transfer region to the electrostatic energy analyser.

The EQS 1000 uses a 45° sector field electrostatic energy analyser (3) consisting of two cylindrical plates with inner and outer radii of 68 and 82 mm, respectively and is preceded by a dc quadrupole lens to correct for the different focal lengths of the sector analyser in the *x*- and *y*-axes. The energy filter has an approximately constant transmission and energy resolution within the energy ranged up to 1000 eV. At the typical passing energy of $E_a = 80$ eV the pass band ΔE_a is less than 3.0 eV full-width at half maximum (FWHM). By decreasing the pass energy, this parameter may be reduced further to about 0.24 eV, but this is accompanied by a corresponding drop in the analyser's transmission.

The energy-separated ions pass down the quadrupole mass filter (4) with a constant energy (about 3 eV) relative to the quadrupole, which is floated at the reference potential (Fig. 1). Ion-trajectory calculations performed by the SIMION 3D code [21] have revealed that the passing conditions are approximately identical for secondary ions with a given *m*/*z* ratio over a wide energy range studied in this work. The quadrupole is a precision assembly (9 mm pole diameter) triple filter with a product of $F \times L$ equal to 51, where F is the working frequency in megahertz, and

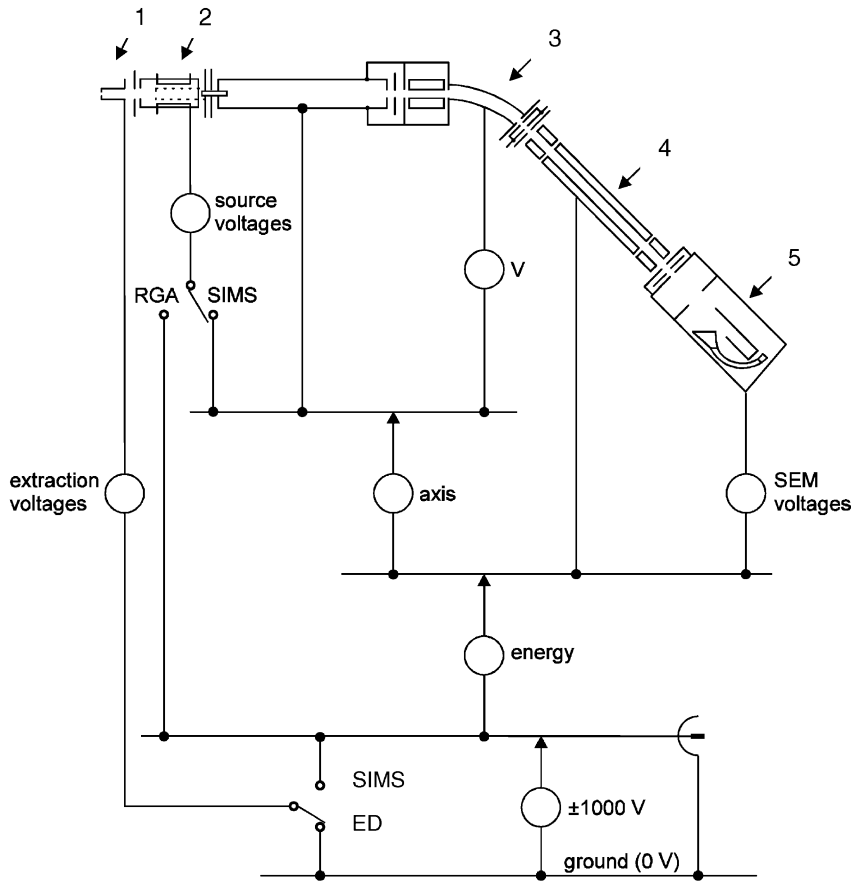

Fig. 1. Schematic configuration of the Hiden EQS 1000 Mass–Energy Analyser: (1) extraction optics; (2) internal ionisation source; (3) electrostatic energy analyser; (4) quadrupole mass filter; (5) secondary electron multiplier.

L is the main filter length in centimetre. The mass resolution ΔM is ca. 0.75 ± 0.05 amu (FWHM) in the mass interval between 1 and 1000 amu.

The EQS 1000 employs an ion-counting secondary electron multiplier (5) with additional first dynode for ion-to-electron conversion. The potential of this electrode (acceleration potential for the registered ions) is adjusted on the level of the signal saturation (about -1000 V for positive ions). Appropriate precautions against detector saturation effects [22] are undertaken.

The EQS MASsoft control software allows flexible control of the probe via the construction of "scan trees". The voltages of the main electrodes (Fig. 1) can be optimised by means of the autotuning procedure to yield the maximum signal intensity. A graphical interface is used to directly build scan structures, which may scan or measure any variable in the system such as *mass*, *energy*, *sample current*, etc. A scan may be a mixture of any operating modes (ED measurements, SIMS, MARISS and RGA) and up to 300 different scans may be included in one single scan cycle.

The analytical chamber is equipped with two primary ion sources featuring separate differential turbo molecular pumps: a mass-filtered duoplasmatron ion gun (model DP50B by VG Fison) generated an O_2^+ ion beam and an electron-impact ionisation source IQE 12/38 by SPECS [23], which provided an inert gas (Ne^+ and Ar^+) ion beam. In our experiments, the projectiles were directed at an angle of incidence of 30°

with respect to the surface plane for both primary ion sources, and secondary ions are measured in the normal direction to the sample surface.

The analytical chamber is evacuated by a turbo molecular pump. The pressure in the chamber was typically 5×10^{-10} mbar. Partial gas pressure was controlled by using the RGA mode. During experiments, the pressure of the working gases was maintained at the level of $(3–5) \times 10^{-9}$ mbar.

The samples probed were pure polycrystalline Mg (99.95%) and Al (99.999%) foils manufactured by Goodfellow [24]. The samples were initially prepared by mechanical polishing and then rinsed with ethanol. After introduction to the analytical chamber, the target surfaces were cleaned by ion-beam sputtering at 0.2–0.5 mA/cm^2 for 10–15 h. The surface conditions were defined by the secondary ion mass spectra. Even after extensive sputtering, some positive and negative impurity ions, especially for the Mg samples, were detected in the secondary ion mass spectra. Here, the samples were considered as "ready for ED investigations", when the ratio of the $^{23}Na^+$ and $^{39}K^+$ mass peak intensities to the $^{27}Al^+$ (or $^{24}Mg^+$) mass peak intensities had decreased by a factor 10 or more (for example, from 0.1 down to 0.005 for $^{39}K^+/^{27}Al^+$ mass peak intensity ratio measured for Ne^+ primaries at 15 eV secondary ion energy), and ceased to change under further ion-beam treatment.

Mass-resolved energy spectra of the secondary ions were measured using a digital scan mode with 0.5–2.0 eV energy step and 0.1–0.5 s dwell time. The accuracy of the energy scale is limited by the uncertainty in the contact potential between the sample and the detector. We estimated this uncertainty to be less than ±0.5 eV.

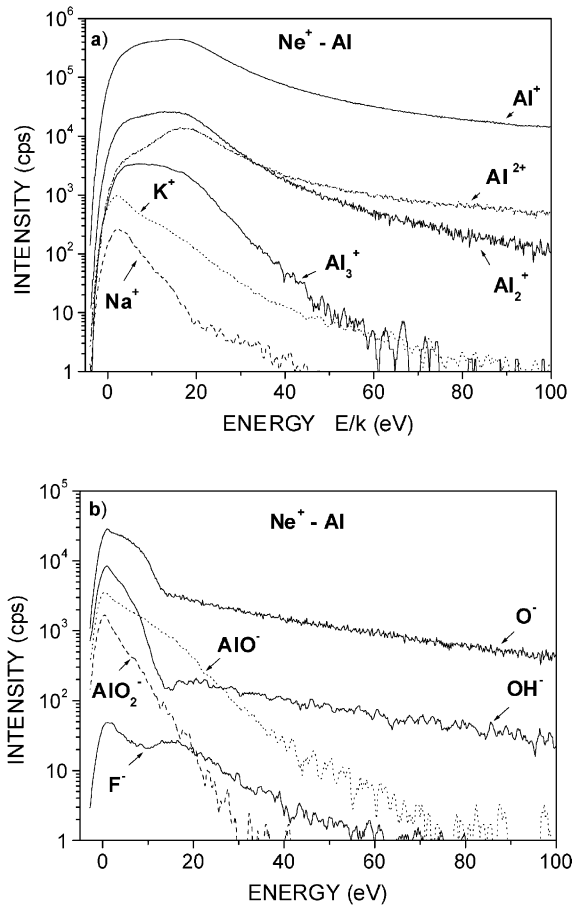

Fig. 2. Energy distributions of the secondary ions sputtered from the Al sample by Ne^+ primary ions ($E_0 = 5$ keV, $I_0 = 2\,\mu$A, rastering 1.5 mm × 1.5 mm, 75% electronic gating): (a) positive ions; (b) negative ions. Parameter k stands for the charge state of the positive secondary ions.

3. Results and discussion

The kinetic energy distribution curves measured under steady-state conditions for essential ion species (positive and negative) sputtered from the Al sample by 5 keV Ne^+ and O_2^+ (2.5 keV per atom) primary ions are shown in Figs. 2 and 3; the results for the Mg sample are presented in Figs. 4 and 5. The EDs of the secondary ions resulting from 5 keV Ar^+ bombardment of both samples were similar in many respects to those measured for Ne^+ primaries, and are not shown here. The intensity of the spectra have not been corrected for the efficiency of the channel electron multiplier, which was approximately constant in the investigated energy range, but not the same for differing positive and negative secondary ions. All measurements have been carried out at a current density less than 100 μA/cm^2.

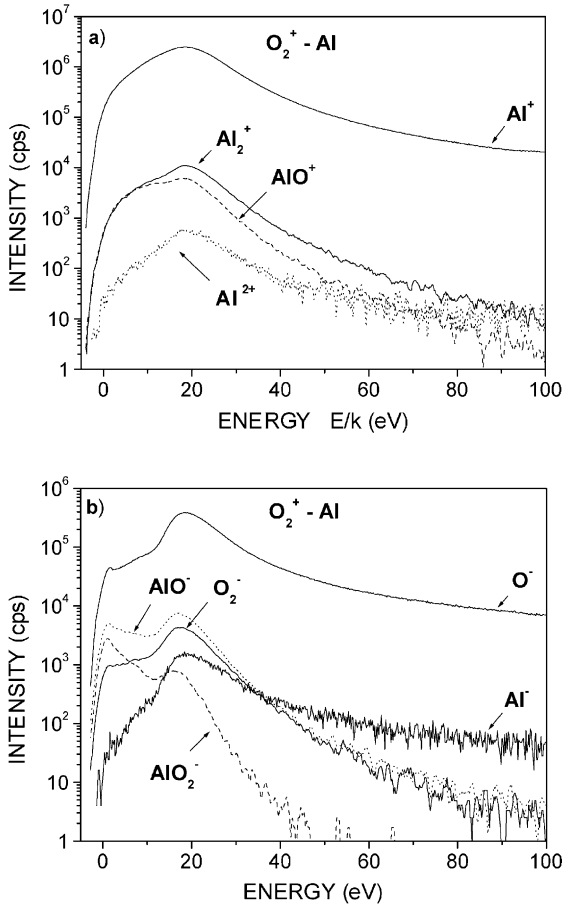

Fig. 3. Energy distributions of the secondary ions sputtered from the Al sample by O_2^+ primary ions ($E_0 = 5$ keV, $I_0 = 0.25\,\mu$A, rastering 0.6 mm × 0.6 mm, 75% electronic gating): (a) positive ions; (b) negative ions. Parameter k stands for the charge state of the positive secondary ions.

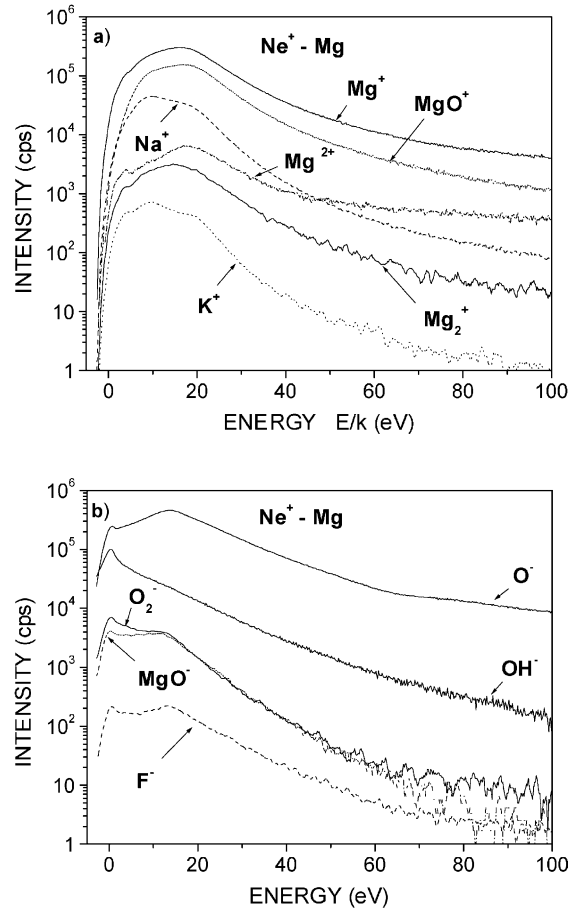

Fig. 4. Energy distributions of the secondary ions sputtered from the Mg sample by Ne^+ primary ions ($E_0 = 5$ keV, $I_0 = 2\,\mu$A, rastering 1.5 mm × 1.5 mm, 75% electronic gating): (a) positive ions; (b) negative ions. Parameter k stands for the charge state of the positive secondary ions.

The main characteristics of the measured EDs are summed up in Tables 1 and 2. Here, the most probable energy, E_{mp}, represents the energy corresponding to the peak in the distribution, the $\Delta E_{0.5}$ is the FWHM, and the E_{avr} is calculated as a mean energy over the range of 0–100 eV.

Usually, an interpretation of ED data is based on the assumption that the sputtering and ionisation (neutralisation) processes responsible for secondary-ion formation are independent of each other, and the energy (velocity) dependence of ionisation (ion survival) probability of secondary ions can be extracted from the explored energy distribution by means of a dividing (or deconvolution) of the theoretical energy spectrum of sputtered neutrals and instrumental functions. This approach is currently being debated [13], but in any case, it presently remains the basis for describing secondary ion yield. We abstain from argument about this concept and concentrate our attention on the experimental findings and on the artefacts, which may influence these findings.

Table 1
Most probable energies E_{mp} (eV), average energies E_{avr} (eV) and full-widths at half-maximum $\Delta E_{0.5}$ (eV) of the EDs of positive and negative secondary ions sputtered from the Al sample by 5 keV Ne^+, Ar^+ and O_2^+

Secondary ions		Ne^+			Ar^+			O_2^+		
m/z	Ion	E_{mp}	E_{avr}	$\Delta E_{0.5}$	E_{mp}	E_{avr}	$\Delta E_{0.5}$	E_{mp}	E_{avr}	$\Delta E_{0.5}$
27	Al^+	14.5	23	22	13	26	25.5	18.5	22	16
13.5	Al^{2+}	33	52	34	29	53	41	35.5	51	25
54	Al_2^+	12.5	17	19.5	10.5	16	17.5	18.5	19.5	14
81	Al_3^+	9.5	12	18	6.0	11.5	14	–	–	–
43	AlO^+	–	–	–	–	–	–	17.5	16.5	18
23	Na^+	2.2	6.2	7.5	1.5	2.6	4.5	–	–	–
39	K^+	2.5	9	7.8	2.0	9	8	–	–	–
27	Al^-	–	–	–	–	–	–	18.5	30	12.5
43	AlO^-	0.5	7.7	8.3	1.8	6.8	7.2	17[a]	14.5	10[a]
59	AlO_2^-	0.5	3.5	4.8	1.5	3.6	5	16[a]	8	10[a]
16	O^-	1	16	9.5	3.6	11	7.5	18.5[a]	26	11.5[a]
32	O_2^-	–	–	–	–	–	–	17[a]	18	10.5[a]
17	OH^-	0.8	8	5.5	2.2	10	5.5	–	–	–
19	F^-	1[a]	16	7.7[a]	1.3	14.5	8.5	–	–	–

[a] Two distinct peaks were observed, and the numbers are presented for the major peak.

Our discussion will start with the positive secondary ion energy distributions presented in Figs. 2a–5a. First, we consider the EDs of the ion species (atomic, cluster, etc.) of the main components of the samples. Almost all of the curves have flat tops, especially for inert primaries. The positions of the peaks, i.e., the most probable energies E_{mp}, are shifted towards higher energy in comparison with commonly observed values (less than 6–8 eV) with extracting fields (see, e.g. [3,5,25–30]). Also, the E_{mp} energies evaluated in our experiments (Tables 1 and 2) are noticeably greater than theoretical values

Table 2
Most probable energies E_{mp} (eV), average energies E_{avr} (eV) and full-widths at half-maximum $\Delta E_{0.5}$ (eV) of the EDs of positive and negative secondary ions sputtered from the Mg sample by 5 keV Ne^+, Ar^+ and O_2^+

Secondary ions		Ne^+			Ar^+			O_2^+		
m/z	Ion	E_{mp}	E_{avr}	$\Delta E_{0.5}$	E_{mp}	E_{avr}	$\Delta E_{0.5}$	E_{mp}	E_{avr}	$\Delta E_{0.5}$
24	Mg^+	15.8	21	18.5	12.5[a]	21	15[a]	18.5	20.5	13.5
12	Mg^{2+}	36	56	35.5	34[a]	64	40[a]	38	54.5	23
48	Mg_2^+	14.2	19	17.5	11.2[a]	17.5	13.5[a]	18.5	21.5	12
40	MgO^+	17	21	18	14	21	16.8	17.5	20.5	15.5
56	MgO_2^+	–	–	–	–	–	–	17.2[a]	16.5	19.5[a]
23	Na^+	10	15.5	16	10.5	15.5	14	16.5[a]	15.5	21[a]
39	K^+	10	14	17.5	8.5	13	16.5	16.8[a]	14.5	20.5[a]
40	MgO^-	9[a]	11.2	22[a]	0.1[a]	8.7	15[a]	17.5[a]	15.8	9[a]
56	MgO_2^-	–	–	–	–	–	–	1.8[a]	12	6.5[a]
16	O^-	13.4[a]	21	20[a]	10[a]	20.5	14[a]	18[a]	23	12[a]
32	O_2^-	0.6[a]	10	9.5[a]	0.1[a]	8.2	15[a]	16.2[a]	13.5	11.5[a]
17	OH^-	0.4[a]	10.5	6.3[a]	0.1[a]	12	15[a]	17.6[a]	18	11[a]
19	F^-	13.2[a]	16	14[a]	9[a]	15	21[a]	17.2[a]	20	11[a]

[a] Two distinct peaks were observed, and the numbers are presented for the major peak.

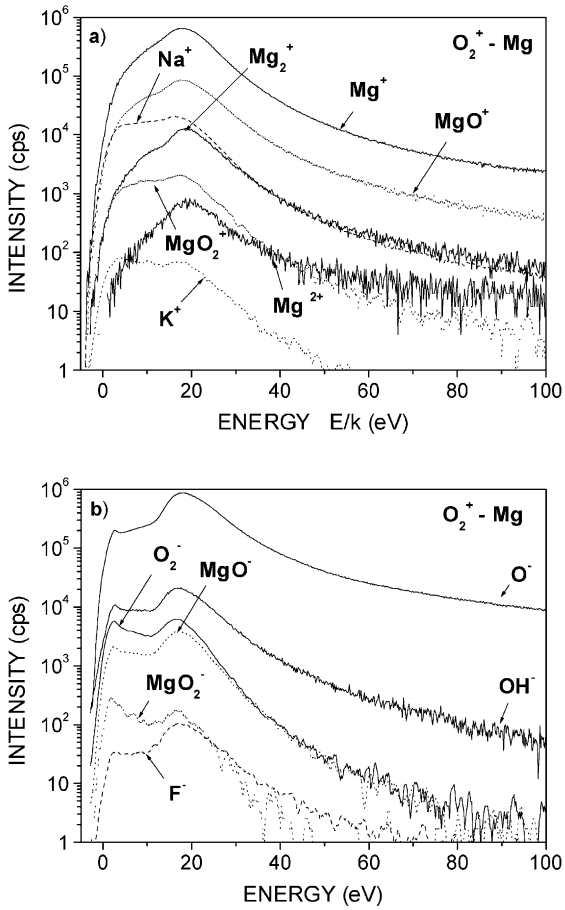

Fig. 5. Energy distributions of the secondary ions sputtered from the Mg sample by O_2^+ primary ions ($E_0 = 5$ keV, $I_0 = 0.25$ μA, rastering 0.6 mm × 0.6 mm, 75% electronic gating): (a) positive ions; (b) negative ions. Parameter k stands for the charge state of the positive secondary ions.

predicted by the Thompson formula (collision cascade theory [31]) for the sputtered neutrals. At this stage, no corrections of the kinetic energy for the image potential or for the other surface barrier energies [32–35] have been carried out, but the reader should be aware that such procedure might increase experimental numbers by a few eV.

The data obtained for Ar^+ primary ions (Tables 1 and 2) are lower than similar data resulting from Ne^+ bombardment. Presumably, not only linear cascade mechanism [31], but also single knock-on collisions (see, e.g. [7,36]) have an influence on the ED peak, and different conditions of the energy transfer under the impact of Ne^+-to-Al (Mg) and Ar^+-to-Al (Mg) cause the difference in the most probable energies and other ED parameters. The coefficient γ, i.e., the maximum portion of a primary energy imparted to a target atom in a binary elastic collision with an incident ion, can be estimated [36] as $\gamma = 4MM_0(M_0 + M)^{-2}$, where M and M_0 stand for the mass of a surface atom and a primary ion, respectively. By this formalism, γ is equal to 0.978 (0.992) for Ne^+-to-Al (Mg) and 0.962 (0.941) for Ar^+-to-Al (Mg) combinations. Changing the primary energy, E_0, from 5 keV to 500 eV reduces the E_{mp} values for the Al^+ secondary ion distribution, namely, from 14.5 to 9.6 eV for Ne^+ primary ions and from 13 to 9.2 eV for Ar^+. Similar results have been obtained for the Mg sample. Under O_2^+ bombardment a reduction of the E_{mp} values with decreasing E_0 have also been observed, but to a lesser extent.

For positive cluster ion, emission from both Mg and Al targets, all energy parameters presented in Tables 1 and 2 monotonically decrease as the size of the clusters increases.

An energy power dependence of the type E^{-s} for the atomic ion species, which could approximate the experimental curves at energies $E_{mp} < E < 70$–80 eV with correlation coefficients of ca. 0.985–0.995, corresponds in general terms to that predicted by the cascade collision theory [31] for the sputtered neutrals, namely, E^{-2}. They display an increase in the value of s with the number n of atoms in the ion, e.g., from 2.3 for Al^+ up to 5.0 for Al_3^+ under Ne^+ ion-beam bombardment of Al sample.

In principle, both of these dependences have been known for long, especially for EDs of the positive silicon secondary ions measured under ion-extracting regime [37,38], but data published for the Al and Mg samples are rather contradictory [5,6,26,27]. For O_2^+ primaries, the energy distributions shown in Figs. 3a and 5a tend to peak at higher energy than for inert ions due to the different mechanism of secondary-ion formation under reactive gas bombardment [39], which causes a stronger dependence of the ionisation probability vs. the energy. For this reason, the $\Delta E_{0.5}$

numbers are smaller, and the reductions in intensities of the EDs with energy are faster for all secondary ions monitored under O_2^+ bombardment (e.g., $s \sim 3.5$ for Al^+ ions).

It is of interest to examine how the *s*-parameter changes within a wide energy range, $E_{mp} < E < 1000$ eV (Fig. 6). Independently of the nature of the primary ions, three sub-ranges with differing slope *s* of the energy power dependence E^{-s} can be marked out for the both samples. The behaviour of the *s*-parameter in the first of them, that is a moderate energy between 20 and 80 eV, has been described before. The second sub-range, $E \sim 80$–250 eV, demonstrates considerable decreasing of the EDs slopes, by about of a factor 2 in comparison with the first range. The third sub-range ($E > 400$ eV) is characterised by very fast drop of the ion intensities vs. the energy and, respectively, by a rise of the EDs slopes ($s \geq 4$). Taking into consideration that EDs of the sputtered neutrals have to depend on energy as ca. E^{-2} [31], we need to suggest that ionisation (ion survival) probability very largely affects our experimental curves and differing ionisation (or neutralisation) mechanisms [39–41] should predominate in the aforesaid sub-ranges. Recently, similar experimental results have been obtained with extracting fields for positive and negative Cu secondary ions [42]. More complicated EDs, with two (low- and high-energy) maxima, were measured by Koval and co-workers [8–10] under 18–25 keV Ar^+ bombardment of different clean and oxidised metal targets (without extracting ions into the mass–energy analyser). Detailed discussion of ionisation phenomena responsible for secondary-ion formation (or survival) is beyond the scope of this paper. The current status of ionisation theories is summed up in a review [13], which states at the end that the "understanding of the mechanism of ion formation in sputtering is still at a very rudimentary stage."

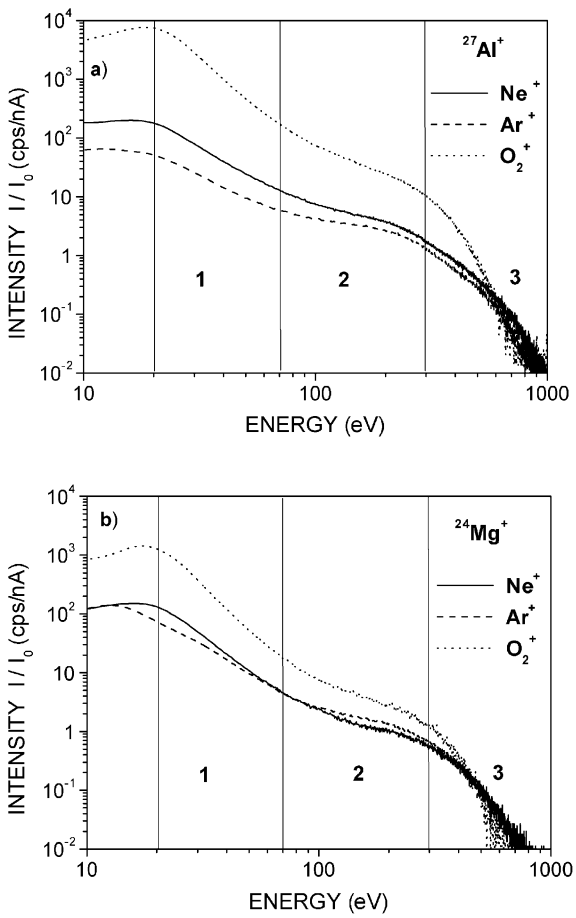

Fig. 6. Normalised energy distributions of the main positive atomic ions resulting from 5 keV ion bombardments of Al (a) and Mg (b) samples. The values of the *s*-parameter estimated for the different energy ranges, marked as (1), (2) and (3) in the figure, are from the followings: (a) Al sample (Ne^+—2.3, 1.1, 4.1; Ar^+—1.9, 0.7, 4.0; O_2^+—3.5, 1.8, 5.8); (b) Mg sample (Ne^+—2.8, 0.9, 3.9; Ar^+—2.2, 0.8, 4.2; O_2^+—4.2, 1.2, 5.8).

Doubly charged positive ions were registered for all combinations of the primary ion-to-sample. The ED parameters for the doubly charged ions surpass the similar parameters for the singly charged ions (see Tables 1 and 2), but the slope *s* of the ED curves are independent of the ion charge, which is in agreement with results formerly obtained with extracting potentials [27,28,43,44].

As mentioned above, the alkaline ions (Na^+ and K^+) are also presented in our spectra. For the Al sample their intensities (Fig. 2a) are small, and the E_{mp} parameters are close to zero energy, clearly pointing to the surface origins of the contaminations. The certified bulk purity of the magnesium was low, namely 99.95% against 99.999% for the aluminium, and more

intensive EDs of alkaline ions were registered for this sample (Figs. 4a and 5a). In our opinion, these EDs are a superposition of the two differing energy spectra: one of them is caused by alkaline impurities adsorbed on the surface (as in the case of the Al sample), and another distribution originates from initial (bulk) contaminations with bigger binding energy. As a consequence, the E_{mp}, E_{avr} and $\Delta E_{0.5}$ data evaluated for Na^+ and K^+ alkali metal ions emitted from the Mg target are greater than the ones obtained for Al (see Tables 1 and 2). Insufficient cleanliness of the Mg samples also results in a marked emission of MgO^+ ions under inert gas ion bombardment (Fig. 4a). For the Al samples, the positive molecular ions such as AlO^+ were measured only under reactive O_2^+ beam bombardment (Fig. 3a).

Energy distributions of the negative secondary ions are presented in Figs. 2b–5b; with almost all of them being initiated by different types of oxygen-containing impurities. To anticipate an expected criticism, we point out that all data presented here were obtained after long-continued and thorough surface cleaning procedures with close control of vacuum and surface conditions by sensitive mass-spectrometric techniques. In spite of these precautions, the thin oxide layers that formed on the Al and Mg surfaces during exposure to air (or during electropolishing treatment) have not been removed completely. The preparation of atomically clean surface of active metals, such as Al and Mg, on the level of SIMS sensitivity is a real challenge [45]. The monitoring of surface contaminations by Auger or ion scattering spectroscopies, frequently used in many studies, especially devoted to ion induced electron emission processes (see, e.g. [46]), does not guarantee the surface cleanness due to the low elemental sensitivity of these techniques.

Energy distributions of the negative secondary ions emitted from the Al sample under inert gas ion bombardment culminate near zero energy (Fig. 2b). The EDs resulting from O_2^+ beam bombardment reveal pronounced double-peak structure (Fig. 3b): one of the peaks is located near zero energy too, and another peak stands at an energy position approximately corresponding to that for positive secondary ions (Fig. 3a). A similar double-peak structure was measured for the Mg sample both for inert and reactive gas bombardment (Figs. 4b and 5b). We think that the low-energy peak is caused by surface adsorbed contaminations, and the other peak is generated by the ions emitted from oxide layers, residual or induced by O_2^+ beam bombardment, with bigger binding energy. On the other hand, we cannot completely rule out an influence on the low-energy peak of stray electric fields, which can exist in any vacuum chamber.

It is interesting to compare the EDs of the same, but oppositely charged ions measured in identical experimental conditions, for example, $Al^{+(-)}$ and $AlO^{+(-)}$ resulting from O_2^+ bombardment of the Al sample (Fig. 3, Table 1). The most probable energy demonstrates independence of the charge state for both ion species; the slope s is bigger for positively charged ions, namely, 3.4 (Al^+) against 2.4 (Al^-) and 5.2 (AlO^+) against 4.5 (AlO^-). The clear tendency of the E_{avr} and $\Delta E_{0.5}$ modification vs. the charge of the ion is not revealed, probably due to the large difference in the shape of the EDs.

4. Summary

We studied in detail the energy distributions of positive and negative secondary ion species produced by 5 keV Ne^+, Ar^+ and O_2^+ ion bombardment of polycrystalline aluminium and magnesium targets. The measurements have been carried out in a small solid angle along the normal to a surface, without any extraction of the ions toward the mass–energy analyser. The essential parameters and features of the spectra were accurately evaluated and tabulated. The main results are summarised in brief as follows.

1. The energy distributions of positive ions peaked at energies higher than commonly observed values for Al and Mg samples under measurements using extraction fields. The most probable energies were found to be different for the inert and reactive primaries; they depended on the primary energy and on the target-to-projectile mass ratio

(for Ne^+ and Ar^+). It indicates that not only linear cascade mechanism, but also single knock-on collisions contribute to the ED peaks.

2. Complicated, non-monotonic dependence of the secondary ion intensity versus the energy was found within a wide energy range $E_{mp} < E <$ 1000 eV. Three energy sub-ranges with different parameter s of the energy power dependence E^{-s} were revealed for energy distributions of Al^+ and Mg^+ ions. With a large degree of probability this means that different ionisation mechanisms were responsible for secondary-ion formation (or survival) into the marked sub-ranges.
3. Nearly all of the negative ion energy spectra were produced by oxygen-containing impurities. They demonstrated complex structure, with two distinct maxima. We are inclined to think that such structure arises from a difference in surface binding energy of the species produced these peaks.

In conclusion, we are aware that our investigation has been devoted to a problem, which has been studied many times. But, we hope that the data presented in this work contain some new information, which can promote a better understanding of sputtering and ionisation processes occurring on the surface under keV ion-beam bombardment.

Acknowledgements

Progetto Finalizzato MSTA II, funded by the National Research Council of Italy, financially supported the work. Useful discussion with M. Karolewski and Z. Šroubek are gratefully acknowledged. We thank M. Buckley for assistance in the preparation of our manuscript.

References

[1] W.O. Hofer, in: R. Behrisch, K. Wittmaack (Eds.), Sputtering by Particle Bombardment III. Characteristics of Sputtered Particles, Technical Applications, Springer, Berlin, 1991, p. 15.
[2] A. Benninghoven, C. Plog, N. Treitz, Int. J. Mass Spectrom. Ion Phys. 13 (1974) 415.
[3] K. Wittmaack, Surf. Sci. 53 (1975) 626.
[4] K.J. Snowdon, R.J. MacDonald, Int. J. Mass Spectrom. Ion Phys. 28 (1978) 233.
[5] M.A. Rudat, G.H. Morrison, Surf. Sci. 82 (1979) 549.
[6] S.P. Chenakin, On some regularities of secondary-ion energy distributions, Preprint IMP 16–90, Kiev, 1990 (in Russian).
[7] L. Wang, R.M. Nor, W.G. Graham, J. Phys. D: Appl. Phys. 30 (1997) 2379.
[8] A.G. Koval, Vacuum 44 (1993) 939.
[9] A.G. Koval, V.A. Litvinov, in: A. Benninghoven, B. Hagenhoff, H.W. Werner (Eds.), Proc. SIMS X, Wiley, Chichester, 1997, p. 259.
[10] V.A. Litvinov, A.G. Koval, S.V. Gritsaenko, Poverchost' N1 (1997) 41 (in Russian).
[11] M.A. Karolewski, R.G. Cavell, Surf. Sci. 480 (2001) 47.
[12] K. Wittmaack, Vacuum 32 (1982) 65.
[13] K. Wittmaack, Surf. Sci. 429 (1999) 84.
[14] A. Tolstogouzov, S. Daolio, C. Pagura, Surf. Sci. 441 (1999) 213.
[15] A. Tolstogouzov, S. Daolio, C. Pagura, C.L. Greenwood, Surf. Sci. 466 (2000) 127.
[16] A. Tolstogouzov, S. Daolio, C. Pagura, Nucl. Instrum. Meth. B 183 (2001) 116.
[17] Hiden Analytical Ltd., 420 Europe Boulevard, Warrington WA5 7UN, England.
[18] J. Kubišta, Z. Dolejšek, Z. Herman, Eur. Mass. Spectrom. 4 (1998) 311.
[19] C. Mair, T. Fiegele, F. Biasioli, Z. Herman, T.D. Märk, J. Chem. Phys. 111 (1999) 2770.
[20] V. Grill, J. Shen, C. Evans, G. Cooks, Rev. Sci. Instrum. 72 (2001) 3149.
[21] D.A. Dahl, SIMION 3D Version 6.0 Users Manual INEL-95/0403, Princeton Electronics Systems, Princeton, NJ, USA.
[22] I.D. Hutcheon, J.T. Armstrong, G.J. Wassenburg, Geochim. Cosmochim. Acta 51 (1987) 3175.
[23] SPECS Gmbh, Voltastraße 5, Berlin D-13355, Germany.
[24] Goodfellow Cambridge Ltd., Ermine Business Park, Huntington PE29 6WR, UK.
[25] G. Slodzian, Surf. Sci. 48 (1975) 161.
[26] K. Wittmaack, Surf. Sci. 429 (1979) 668.
[27] G. Blaise, A. Nourtier, Surf. Sci. 90 (1979) 495.
[28] R.-L. Inglebert, J.-F. Hennequin, J. Microsc. Spectrosc. Electron. 7 (1982) 257.
[29] J.-F. Hennequin, J.-L. Bernard, Surf. Sci. 234 (1990) 127.
[30] S.A. Larson, L.L. Lauderback, Phys. Rev. B 43 (1991) 36.
[31] M.W. Thompson, Philos. Mag. 18 (1968) 377.
[32] M.J. Vasile, Phys. Rev. B 29 (1984) 3785.
[33] M.J. Vasile, Nucl. Instrum. Meth. B 40/41 (1989) 282.
[34] B.J. Garrison, Surf. Sci. 167 (1986) L225.
[35] M.L. Yu, Rad. Effects Def. Solids 109 (1989) 259.
[36] W. Eckstein, Nucl. Instrum. Meth. B 27 (1987) 78.
[37] K. Wittmaack, Phys. Lett. 69A (1979) 322.
[38] S.N. Schauer, P. Williams, Int. J. Mass Spectrom. Ion Phys. 103 (1990) 21.

[39] M.L. Yu, in: R. Behrisch, K. Wittmaack (Eds.), Sputtering by Particle Bombardment III. Characteristics of Sputtered Particles, Technical Applications, Springer, Berlin, 1991, p. 91.
[40] Z. Šroubek, Spectrochim. Acta 44B (1989) 317.
[41] D.V. Klushin, M.Y. Gusev, S.A. Lysenko, I.F. Urazgil'din, Phys. Rev. B 54 (1996) 7062.
[42] P.A.W. van der Heide, Nucl. Instrum. Meth. B 157 (1999) 126.
[43] Z. Jurela, B. Perovič, Can. J. Phys. 46 (1968) 773.
[44] G. Blaise, G. Slodzian, Rev. Phys. Appl. 8 (1973) 105.
[45] R.G. Musket, W. McLean, C.A. Colemenares, W.J. Siekhaus, in: A.W. Czanderna, C.J. Powell, T.E. Madey (Eds.), Specimen Handling, Preparation, and Treatments in Surface Characterization, Kluwer Academic Publishers, New York, 1998, p. 63.
[46] P. Riccardi, P. Barone, M. Camarca, A. Oliva, R.A. Baragiola, Nucl. Instrum. Meth. B 164/165 (2000) 886.